Materials Today Communications 33 (2022) 104290

Contents lists available at ScienceDirect

Materials Today Communications

journal homepage: www.elsevier.com/locate/mtcomm

A facile surfactant-free strategy to construct porous structures with hydrophobic and hydrophilic domains from polymer/water mixtures

Alessandra Partenope [a,1], Fabio Pizzetti [a,1], Valeria Vanoli [a], Mosè Casalegno [a], Alberto Cingolani [b], Liebert Parreiras Nogueira [c], Franca Castiglione [a], Håvard J. Haugen [d], Filippo Rossi [a,*]

[a] Department of Chemistry, Materials and Chemical Engineering "Giulio Natta", Politecnico di Milano, via Mancinelli 7, 20131 Milano, Italy
[b] Department of Chemistry and Applied Biosciences, Institute for Chemical and Bioengineering, ETH Zürich, Vladimir-Prelog Weg 1-5/10, 8093 Zurich, Switzerland
[c] Oral Research Laboratoy, Institute for Clinical Dentistry, University of Oslo, PO Box 1109 Blindern, NO-0317 Oslo, Norway
[d] Department of Biomaterials, Institute for Clinical Dentistry, University of Oslo, PO Box 1109 Blindern, NO-0317 Oslo, Norway

ARTICLE INFO

Keywords:
Colloids
Drug delivery
Nanoparticles
Polymer
Polymerization

ABSTRACT

In Pickering emulsions colloidal nanoparticles can efficiently stabilize water/oil mixtures and has been demonstrated for a wide range of applications. However the low mechanical properties of the final devices are limiting their adoption. Here we propose a strategy to use colloidal nanoparticle at hydrohobic polymer-water interface able to form biphasic, stable and porous structures during monomer polymerization. The final devices present two separate phases with different water affinities that make them extremely promising in many different fields. The strategy described present so high versatility and can be applied to different monomers and nanoparticles opening the doors to diverse applications.

1. Introduction

In the world of formulations made of oil and water emulsions play a pivotal role [1,2]. They have indeed been studied since the 900's and products utilizing this technology has been developed for food, cosmetics and pharmaceutics, among others [2,3]. The concept of emulsion stability is linked to the use of small amphiphilic molecules called tensides (here emulsifiers) that can accumulate at the oil/water interface decreasing the interfacial tension. Although highly efficient, the use of tensides is linked to issues like allergies and toxicity for humans and water pollution [4,5]. In the early twentieth century, Spencer Pickering [6–8] discovered that oil/water mixtures can be stabilized using solid particles. They indeed can accumulate at the interface between the two immiscible liquids preventing coalescence and phase separation [9]. Even though this phenomenon was discovered more than a century ago, it was first recently that it has drawn interest from researchers and industry [10,11]. Indeed the use of solid particles present several advantages: i) the elimination of tensides from formulation, ii) solid particles can be designed in order to add properties to the emulsions like conductivity, porosity etc. [9,12]. It is well known that many types of inorganic (silica, clay and hydroxyapatite among others) and organic particles can be Pickering emulsifiers, opening the field to many different possibilities [8,13]. A particular type of Pickering emulsions is bijels, where the two components (oil and water) are present in similar amount and constitute a bicontinuous system [14,15]. From an application perspective the presence of two separate domains can be advantageous. For example in precision medicine, where different drugs should be administered at different time points with different kinetics, bijels allows for the possibility to deliver both hydrophobic and hydrophilic molecules with a so-called multi-drug delivery strategy [16–18].

Differently from emulsions, in these systems, the amount of drugs (both hydrophilic and hydrophobic) that can be loaded can be high, opening a lot of promising medical possibilities [19]. However the use of bijels is strongly limited by their inadequate mechanical properties and the use of tensides is necessary to stabilize these systems [14,20].

Moreover one of the key point is represented by porosity, very important material-related property [21,22]. The success in multiple applications does indeed require adequate porosity, such as catalysts, absorbents, drug carriers, combustible production, waste management, micro-electronics, medical diagnosis, among others [23,24]. In this

* Corresponding author.
E-mail address: filippo.rossi@polimi.it (F. Rossi).
[1] These authors equally contributed to this work.

https://doi.org/10.1016/j.mtcomm.2022.104290
Received 20 April 2022; Received in revised form 2 August 2022; Accepted 19 August 2022
Available online 22 August 2022
2352-4928/© 2022 Elsevier Ltd. All rights reserved.

direction recently crystallization-driven gelation was developed with the final aim to build porous polymer networks [25,26]. In this strategy researchers are interested in using water as template to introduce porosity within polymeric phase forming aerogels, used in environmental applications like oil spill cleanup [27]. In this work, taking inspiration both from Pickering emulsions and bijels, we are interested in developing a strategy to build a class of biphasic porous structures where oil and water are present in comparable amount and solid nanoparticles are used to stabilize the final system. The simultaneous presence of water and oil phases can guarantee the possibility to have a system that present different solvent affinities at the same time. Oil phase is constituted by an hydrophobic monomer (ϖ-pentadecalactone, PDL) that can polymerize in bulk together with ethanol as initiator and triazabicyclodecene (TBD) as catalyst [28,29]. The final porous system was characterized and the possibility to load and deliver simultaneously drugs with or without affinity with water investigated.

2. Materials and methods

2.1. Materials

For biphasic porous structure structures synthesis: ω-pentadecalactone (PDL), ethanol and 1,5,7-triazabicyclo[4.4.0]dec-5-ene (TBD) were purchased from Merck (previously Sigma Aldrich Chemie GmbH, Deisenhofen, Germany). For the hydroxyapatite (HA) nanoparticles: calcium hydroxide (Sigma Aldrich Chemie GmbH, Deisenhofen, Germany) and orto-phosphoric acid (Merck, Germany). Fluorophores that have been used as fluorescent drug mimetics in release tests were fluorescein sodium salt, fluorescein isothiocyanate (FITC) and fluorescein-dextrans (MW = 10 kDa and 70 kDa) by Merck, Germany. Products containing fluorescent molecules have been stored at 4 °C in the dark until their use. Fluorescent tracers used for fluorescent confocal microscopy images were doxorubicin and pyrene, both from Merck, Germany. All the aqueous solutions were prepared using *milliQ* water. All reactants and solvents have been used as received, without further purifications. Solvents were of analytical grade. The reactions were carried out under atmospheric pressure.

2.2. Characterization techniques

Fourier transform infrared (FTIR) transmission spectra were recorded using a Thermo Nexus 6700 spectrometer coupled to a Thermo Nicolet Continuum microscope equipped with a 15 × Reflachromat Cassegrain objective at a resolution of 4 cm^{-1} using the ATR technique.

Absorbance was measured by Tecan® Microplate Reader spectrophotometer at the highest excitation wavelength typical of each tracer (fluorescein = 485 nm, DXT = 500 nm), applying the Lambert-Beer equation.

Dynamic light scattering (DLS) measurements were performed with a Malvern Zetasizer Nano ZS at a scattering angle of 173° (backscatter). The temperature was kept at 25 °C and an equilibration time of 60 s was provided before each measurement.

Gel permeation chromatography (GPC) analyses had been carried out using a Jasco LC-2000Plus gel permeation chromatograph coupled with a refractive index detector (RI-2031Plus, Jasco) using 3 Agilent PLgel columns, 5×10^{-6} M particle size, 300 × 7.5 mm (MW range: 5×10^2 to 17×10^5 g/mol). The GPC samples were injected using a Jasco AS-2055Plus autosampler. The instrument was calibrated using polystyrene standards. The analyses had been carried out using tetrahydrofuran (THF) as eluent and a 0.5 mL/min flow rate at a temperature of 35 °C.

X-ray diffraction (XRD) experiments were carried out using a Bruker D2-Phase diffractometer equipped with Cu radiation using Bragg-Brentano geometry. Experiments were performed at room temperature on powders.

Differential scanning calorimetry (DSC) was performed on devices after being lyophilized using a Mettler Toledo DSC: samples were heated from − 60–180 °C at heating rate of 10 °C/min.

2.3. Hydroxyapatite synthesis

HA has been synthesized using a modified version of the procedure proposed by Kumar and coworkers [30]. A solution of $Ca(OH)_2$ 0.2 M (368.8 mg, 10 eq.) in distilled water (24.9 mL) was stirred at 400 rpm at 100 °C for 1 h. Then a 0.12 M solution of H_3PO_4 (0.2 mL, 6 eq.) in distilled water (24.9 mL) was added at a controlled rate of 4 mL/min using a programmable syringe pump. At the end of the addition, the pH was checked to be close to neutrality and the mixture was left reacting for 2 h. After resting overnight, the solution underwent five centrifugation cycles at 5000 rpm for 3 min, with supernatant removal and particles redispersion between each of them. The product was then dried and calcinated in an oven at 200 °C for 6 h. Finally, it was ground in order to obtain the nanoparticles. The overall yield was 94.4% and the hydroxyapatite appeared as a white fine powder. The final product was characterized and its purity tested using powder XRD, achieving good agreement between the obtained pattern and the one reported in reference article [30].

2.4. NPs dispersion

The dispersion has been achieved using the following procedure: a solution of arabic gum (AG) in distilled water was heated at 37 °C for 1 h under moderate stirring. Successively, a known mass of NPs was added to the solution so that the weight ratio between NPs and AG was 1:1 and the desired concentration was reached. The so-formed dispersion was sonicated for 12 h in an ultrasonic bath to make the AG grafted onto the NPs surface. The final NPs dispersion was characterized using DLS, scanning electron microscopy (SEM) and transmission electron microscopy (TEM).

2.5. Biphasic porous structures synthesis

To a mixture of ω-pentadecalactone (8.8 mmol, 1 eq.), ethanol (1.89 mmol, 0.2 eq.), used as an initiator, and a catalytic amount of TBD (0.189 mmol, 0.02 eq.) were added. The solution was mixed in a hot bath, water at T = 80 °C, for 2 h maintaining the stirring at 800 rpm. The reaction was carried out in a round bottom flask and the stirring is maintained with a magnetic stir bar. Then, a precise volume of HA colloidal dispersion in water (20 mg/mL, 1 mL) was introduced, mixing continuously, at least 20 min, until complete polymerization is obtained. The final product was removed as a liquid from the flask with a Pasteur pipette and casted in molds. By solidifying the product at room temperature, a solid and compact structure is formed. Using this method, removing the sample when ready was removed without breaking its structure.

2.6. Drug loading

Due to their dual nature, biphasic porous structures should theoretically be able to entrap both hydrophilic and hydrophobic drug mimetics. The cargo loading was different if the fluorescent tracers were hydrophilic or hydrophobic: as far as the former are concerned, they were dissolved directly in the aqueous solution of NPs, whereas the latter have been added to the caprolactone prior to polymerization.

In all these cases, a concentration of 1 mg/mL has been used. Furthermore, also the fluorescent tracers required for fluorescent confocal microscopy have been added following this procedure.

2.7. Swelling behavior

Biphasic porous structures have been lyophilized immediately after

the synthesis and weighted (w_0). The samples were then immersed in phosphate buffer saline solution (PBS), stored at 37 °C and removed at specific time points to be weighted again (w_t). The timepoints collected were initially more frequent to monitor eventual fast swelling kinetics. The mass swelling ratio (Q_M) had been evaluated using Eq. 1:

$$Q_M = \frac{w_t - w_0}{w_0} \quad (1)$$

The swelling graphs have been plotted along with the standard deviation.

2.8. Drug release experiments

The cargo was loaded during the biphasic porous structure synthesis, furthermore different types of fluorescent molecules have been tested. After the synthesis each sample was submerged in excess of PBS solution (0.1 M, pH 7.4) and stored in an incubator at 37 °C at a controlled level of moisture, resembling human body conditions. At certain time intervals the surrounding liquid was collected for UV analysis. The reading was carried out on 100 μL aliquots repeated three times for every timepoint, in order to avoid any concentration gradient. The PBS taken was then restored fresh one to keep the volume constant. The UV analysis was carried out spectrophotometrically at the characteristic excitation wavelength of each molecule. After this assay, the amount of fluorophore released was evaluated with Eq. 2:

$$\text{Mass released}[\%] = \frac{m^t_{tot}}{m_0} \bullet 100 \quad (2)$$

Where m^t_{tot} is the overall mass released at time t and m_0 is the initial sample mass.

2.9. Fluorescent confocal microscopy

Fluorescent confocal microscopy analyses have been performed introducing a fluorescent tracer inside the biphasic porous structures. Two different molecules have been selected: rhodamine B and pyrene; the former being a hydrophilic tracer, while the latter a hydrophobic one. Images were collected at different magnifications using an Olympus Fv1000 confocal microscope (Laser 594 nm).

2.10. ESEM analysis

Environmental scanning electron microscopy (ESEM) and elemental analysis (EDS) were performed on gold-sputtered samples at 10 kV with Evo 50 EP Instrumentation (Zeiss, Jena, Germany). To preserve the actual morphology of the biphasic porous structures, freeze-drying (for 24 h) was applied to remove all the liquid phase by sublimation. Because of the low operating temperature and pressure, the polymer chains were expected to retain the same conformation they had in wet conditions. Comparative evaluation of the superficial and internal morphology of the investigated samples was carried out.

2.11. Cytotoxicity

Mouse fibroblasts (L929) were cultured in complete medium (Dulbecco' s modified Eagle's medium (DMEM) supplemented with 10% fetal bovine serum, 1% penicillin/streptomycin, 1% L-glutamine 200 mM). Cells were maintained at 37 °C in 5% CO_2 and used. 3D macrostructures were formed and located into cell culture inserts (Falcon, 1.0 μm pore size). L929 were seeded in 24-well plates at a concentration of 50,000 cells/well in 1 mL complete medium and grown at 37 °C, 5% CO_2. After 24 h, the medium was changed and the inserts with biphasic porous structures were added in contact with the medium. After 3 days of culturing, the cytotoxicity of macrostructure was evaluated by performing an MTS assay [31]. The absorbance was measured at 570 nm, and the results were compared with that of the control wells to determine relative cell viability.

2.12. HR-MAS NMR spectroscopy

^{1}H HR-MAS (hig-resolution magic angle spinning) NMR (nuclear magnetic resonance) experiments on a biphasic porous structure sample were performed on a Bruker Avance NEO spectrometer operating at 500 MHz proton frequency, equipped with a dual ^{1}H/^{13}C HR-MAS probe head suitable for semi-solid samples. The sample was loaded in a 4 mm ZrO_2 rotor containing a volume of about 12 μL and a spinning rate of 4 kHz was used to eliminate the dipolar contribution. Self-diffusion coefficients were measured by diffusion ordered correlation spectroscopy (DOSY) experiments by applying sine shaped pulsed magnetic field gradients along the z-direction up to a maximum strength of G = 53.5 G cm^{-1}. The bipolar pulse longitudinal eddy current delay (BPPLED) sequence was applied.The pulse gradients were incremented from 2% to 95% of the maximum gradient strength in a linear ramp with 32 steps. The duration of the magnetic field pulse gradients (δ) and the diffusion times (t_d) were optimized in order to obtain complete dephasing of the signals with the maximum gradient strength. A series of five experiments were performed with t_d in the range (20−50) ms and δ = 3.0–1.4 ms. Each spectrum was acquired with 8 scans, a relaxation delay of 10 s and 32 K points. The ^{1}H DOSY experiments were repeated twice. The temperature was set and controlled at 32 °C with an air flow of 535 l·h^{-1}.

2.13. Nano-computed tomography

All specimens were scanned in a nano-computed tomography (nano-CT) device (SkyScan 2211 Multiscale X-ray Nano-CT System, Bruker micro-CT, Kontich, Belgium) with a 20–190 kV tungsten X-ray source and a dual detection system: an 11-megapixel cooled 4032 × 2670 pixel CCD-camera and a 3-megapixel 1920 × 1536 pixel CMOS flat panel. Prepared roots for cementum analysis were scanned at 38 kV, 370 μA and 1400 ms. The scans were taken over 180° with a rotation step of 0.14° and a voxel size of 800 nm using the CCD detector. Projections were reconstructed using the system-provided software, NRecon (version 1.7.4.6), and analyzed with CTAn (Bruker micro-CT, version 1.18.4.0).

2.14. Statistical analysis

Experimental data were analyzed using Analysis of Variance (ANOVA). Statistical significance was set to p value < 0.05. The results are presented as mean value ± standard deviation.

3. Results and discussion

In this work we develop a surfactant free-strategy strategy for producing mechanically stable biphasic structures without using organic solvents. The procedure involved the use of an hydrophobic monomer that can polymerize in bulk conditions. The monomer indeed undergoes polymerization forming a polymer that is hydrophobic as well. Then, during the addition of colloid (HA NPs in water) the polymerization is stopped by water and the final system is stabilized by hydroxyapatite nanoparticles that can accumulate at the interface giving strong stability to the device. HA NPs were synthesized starting from a solution of Ca $(OH)_2$ then stabilized using arabic gum (characterization details in Supporting Information section). The protocol developed for the formation of the 3D biphasic structure is presented in Fig. 1. The reaction starts at 80 °C for 2 h in a round bottom balloon loaded with PDL, EtOH and TBD (Fig. 1a). The monomer polymerizes though a ring-opening polymerization (Fig. 1b). Then the temperature decreases and, at 50 °C, the water suspension of HA NPs (20 mg/mL) is added and then mixed for 2 min. At the end the material can be removed through a

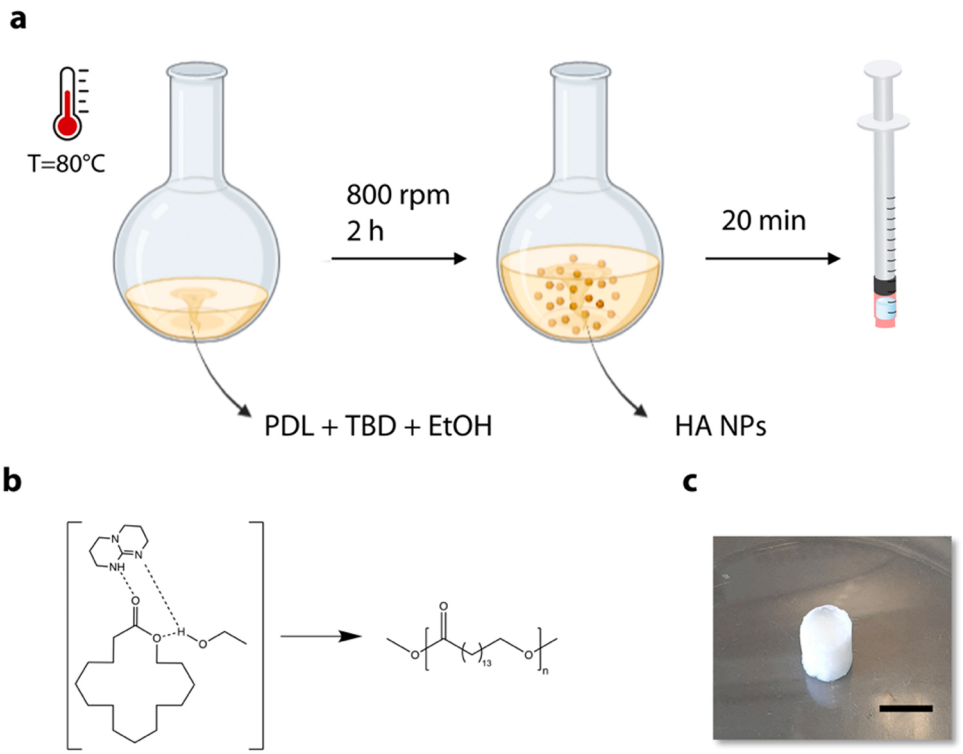

Fig. 1. a) Schematic representation of the steps used for biphasic porous structures production; b) PPDL polymerization mechanism; c) obtainment of biphasic porous structure visible without water loss. Scale bar = 1 cm.

syringe and mold in different shapes (here cylinder, Fig. 1c) without water loss. The time point for addition of the colloidal suspension is fundamental for the final properties of the system: a too late addition will cause phase separation between polymer formed and water, while a too early addition will deactivate the catalyst (TBD) and the polymerization cannot proceed. This time was optimized in this direction (2 h) giving the possibility to build a stable structure able to retain water and polymer together (Fig. 1c).

The final device was then characterized with different analyses. Firstly, FTIR spectrum after many washing cycles (Fig. 2a) revealed the presence of both peaks of PDL, HA NPs and water underlining the stability of their presence not related to unwashed samples. Indeed signal at 2940 cm^{-1} is typical of C-H hydroxyl groups with asymmetric stretching. Also the peak related to the C-H hydroxyl group of aliphatic polymer chains is visible at 2860 cm^{-1}. Then carbonyl groups (1240 cm^{-1}) of the ester and C-O-C stretching (1150 cm^{-1}) present clear signals. The presence of HA NPs is correspondent to band at 1600 cm^{-1} (* in Fig. 2a) and water at 3450 cm^{-1} (** in Fig. 2a).

The polymer was then analyzed with GPC after being dissolved in THF (Fig. 2b). The impact of HA NPs addition, as water suspension, on polymerization was evaluated comparing the two situations: *i*) PPDL in biphasic porous structure (blue line) and *ii*) polymer obtained in the same conditions without NPs addition (black line). From such analysis it is evident that HA NPs only partially affects polymerization. Indeed the average molecular weight of polymer phase in biphasic structures is 1700 Da, the distribution of molecular weights 1.3 and degree of polymerization equal to 6.5. The average molecular weight obtained without NPs addition is 1900 Da, the distribution of molecular weights 1.2 and degree of polymerization equal to 7.5.

Considering that TBD is deactivated by water, it is possible that rapid polymerization occurs at the beginning of the mixing and the remaining reaction time is required to let the structure rearrange without further increase of polymer molecular weight. Moreover we should consider the samples obtained without NPs addition were not able to retain water and phase separation was well visible (Supporting Information).

The DSC thermogram (Supporting Information) of biphasic porous structures shows that there was a small reduction in melting temperature (76 °C) with respect to neat PPDL (79 °C) [32]. This DSC results further confirm both the crystallinity of the biphasic porous structures and the good miscibility between the components present in the structure [33].

The final system cannot be classified as a hydrogel, because of the hydrophobic domains present, but it has similar characteristics [34,35]. In particular, the ability to swell (Fig. 2c) and biocompatibility (Supporting Information) are properties in common with hydrogels [36,37]. The swelling ability, responsible of elastic properties behind hydrogels, is different respect to neat PPDL that, as known, is extremely hydrophobic and not present. Differently from neat polymer, biphasic samples reached swelling equilibrium after 1 h and exhibit superabsorbent behavior.

The biphasic nature of the system was verified using confocal microscopy (Supporting Information): two dyes, one hydrophilic (rhodamine B, red color), and one hydrophobic (pyrene, green color) were used and colocalization of the two signals was not visible. The high porosity of the biphasic system is visible in Fig. 3 from ESEM images of freeze-dried samples. From Fig. 3c Carbon EDS map is visible and corresponds to the polymeric phase while Fig. 3d shows Calcium EDS map that corresponds to HA NPs chemical structure. It is well visible that while polymer phase represents the bulk HA NPs are accumulated at the interface. Moreover, the presence of two distinct phases (oil and water) is highlighted by NMR measurements. Diffusion-ordered spectroscopy (DOSY) can separate different molecular species considering their diffusion coefficient D. The ^{1}H DOSY experiment, acquired with a defined diffusion time t_d and analyzed as 2D map, is shown in Fig. 4. The presence of two distinct domains (oil and water) is visible as it is associated with two distinct values of D.

A conventional analysis of the DOSY experiments [38] relates the signal intensities, $I(q,t_d)$, obtained with increasing pulsed field gradient intensity, with the diffusion coefficient D using the following equation:

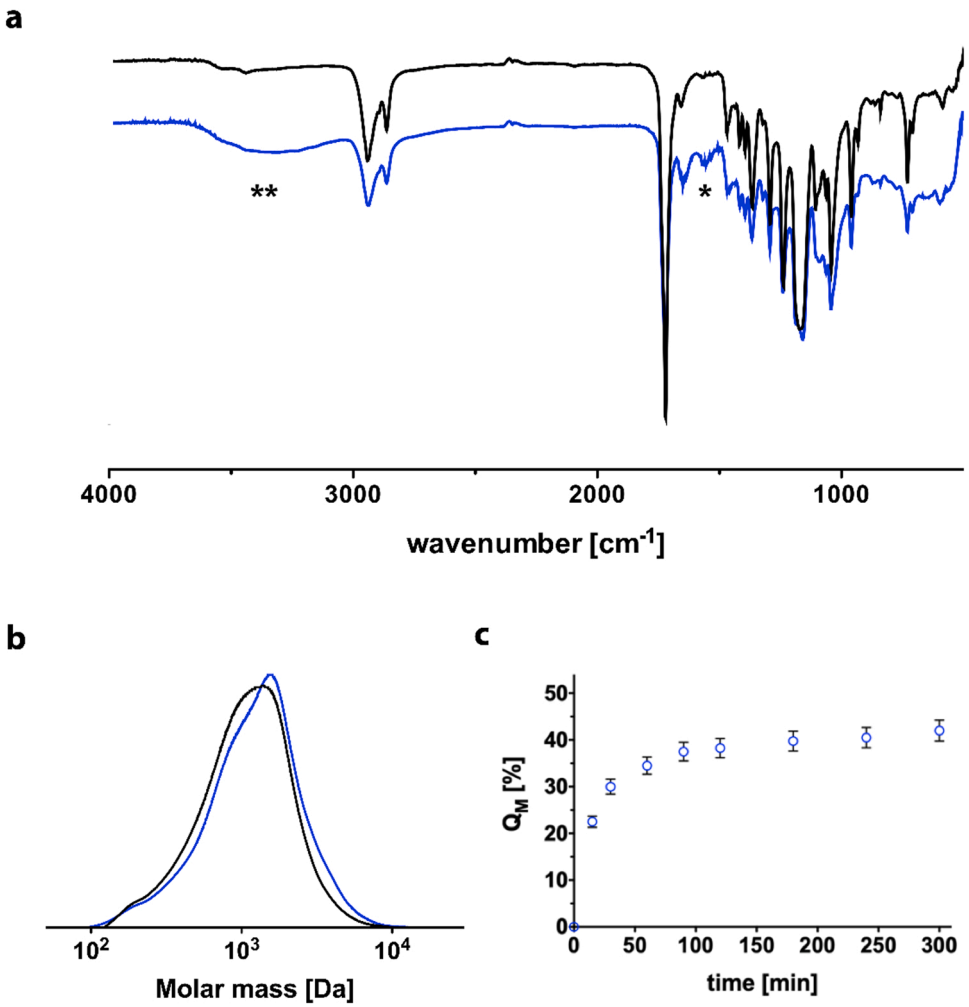

Fig. 2. a) FTIR spectrum of the biphasic porous structures (blue line); b) GPC analysis of PPDL in biphasic porous structures (blue line) and without NPs addition (black line); c) swelling ratio of the biphasic porous structures at neutral pH (n = 3, mean ± standard).

$$I(q,t_d) = I_0(0,t_d) \bullet e^{-q^2 \bullet D \bullet t_d} \quad (3)$$

where $q = (\delta \bullet \gamma \bullet g)/\pi 2$, γ is the giromagnetic ratio of the observed nucleus, δ is the gradient duration and *g* the intensity. This model assumes the probed molecular species to follow Gaussian diffusion, characterized by a single diffusion coefficient D, which is determined via simple linear regression. In our biphasic system, the diffusion coefficient of water molecules is $D = 1.14{\cdot}10^{-9} \pm 0.05{\cdot}10^{-9}$ m^2/s, while the reported D value at 305 K is $2.7{\cdot}10^{-9}$ m^2/s. A slower diffusion of water is observed in this system, which can be explained by the motion restriction of small molecules in a confined system. In order to account for the possibility of non-Gaussian diffusion, the following, more general model was also considered [39]:

$$I(q,t_d) = I_0(0,t_d) \bullet e^{-K \bullet t^{\beta} \bullet q^{\mu}} \quad (4)$$

where K is a generalized diffusion coefficient with dimensions $\left[m^{\mu}s^{-\beta}\right]$. The exponents β and μ are related to α by means of the following equation:

$$\alpha = \frac{2\beta}{\mu} \quad (5)$$

where α is the diffusion exponent. It can be shown that, if the diffusion obeys the Fick's laws, so that α = 1, Eq.(4) simplifies to Eq.(3). Species not following a Fickian diffusive behavior may be expected to show values of α different from one, thereby corresponding to a so-called subdiffusion (0 < α < 1) and superdiffusion (α > 1). Commonly observed subdiffusion is characterized by α < 1 and μ = 2), whereas superdiffusion by α > 1 and μ < 2. Deviations from a Fickian behavior not necessarily imply non-Gaussian diffusion, and vice versa. Thus for example, Fickian, non-Gaussian diffusion may be observed for α = 1, and μ ‡ 2. Fig. 4b shows the raw normalized signal intensities along with the profiles obtained by fitting the parameters α, μ, and K via Eq.(4) [39]. The values of such parameters were as follows: α = 1.02 ± 0.00, μ = 1.69 ± 0.01, and $K = 0.274{\cdot}10^{-7} \pm 0.017{\cdot}10^{-7}$ m^{μ}/s^{β}, thereby suggesting a Fickian and non-Gaussian diffusion of water molecules.

Further analysis on the biphasic structure of the system was conducted with nano-CT technology that allowed us to obtain a 3D reconstruction of the internal structure of the sample and to evaluate the porosity of the system. Fig. 5 shows the reconstruction of the sample where the porosity of the system and their interconnection can be observed (details in Supporting Information). The presence of the two phases is visible from the two colors that represent the polymeric phase (light color) and water phase (dark color).

A favorable feature of these system is the simultaneous loading of drugs with and without water affinity. Generally, in drug delivery systems, hydrohobic drugs can be loaded using emulsions while here the biphasic nature of the system can guarantee the multiple loading and consequent release without interactions between the drugs loaded and oil/water phases.

For this study we used drug mimetics commonly used to represent low molecular weight hydrobilic drugs, low molecular weight

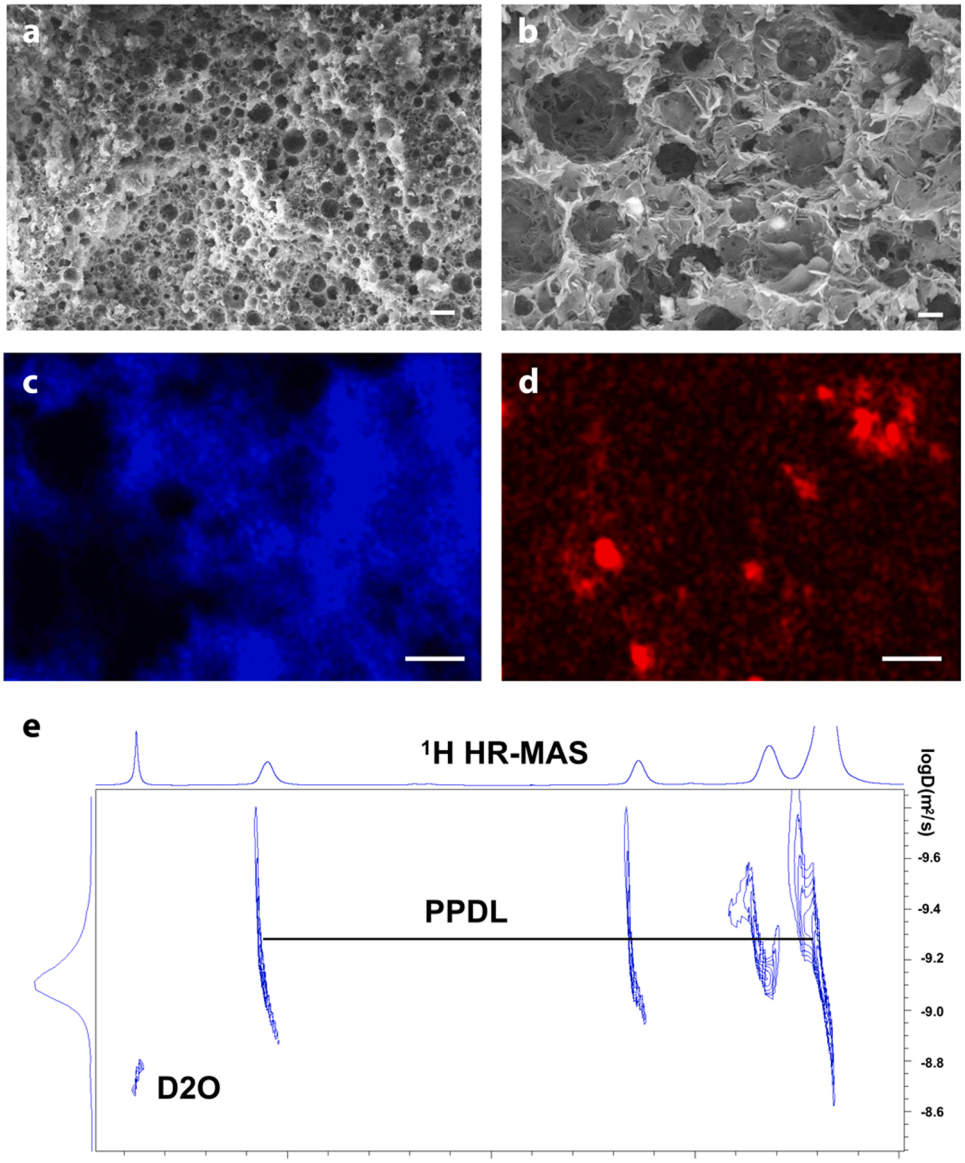

Fig. 3. ESEM images of biphasic structure (scale bars = 50 μm (a), 15 μm (b)); c) EDS image on C presence within the sample (scale bar = 50 μm); d) EDS image on Ca presence within the sample (scale bar = 50 μm).

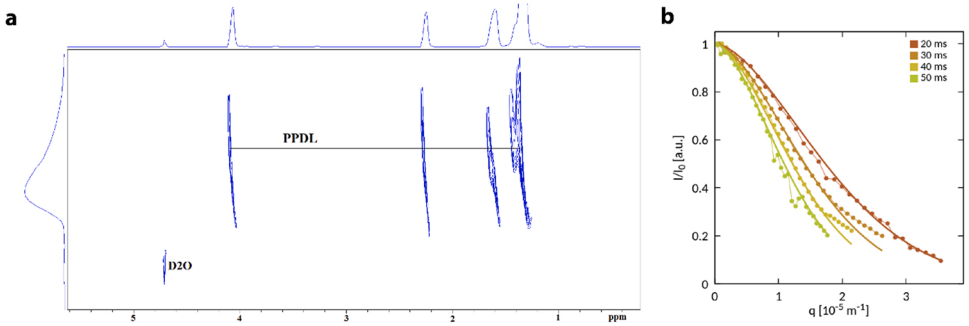

Fig. 4. a) ^{1}H HR-MAS DOSY map of the biphasic porous structure sample. The *x*-axis displays the ^{1}H chemical shift (ppm), while the *y*-axis displays the log(*D*) values (m^2 s^{-1}); b) DOSY-NMR normalized signal intensities as a function of q. Raw data (line-points) are drawn for the diffusion times considered (t_d = 20, 30, 40, and 50 ms). Continuous lines represent the curves obtained by fitting the data via Eq.(4).

hydrobobic drugs and high molecular weight hydrobilic drugs typical of biomolecules [40,41]. Hydrophilic molecules (here sodium fluorescein with different molecular weight) can be loaded together with HA NPs, while hydrophobic (FITC here) with polymer/catalyst/initiator mixture (Fig. 6a, b). This loading procedure ensures maximum loading (100%), higher than in emulsions and without affecting the formation of the

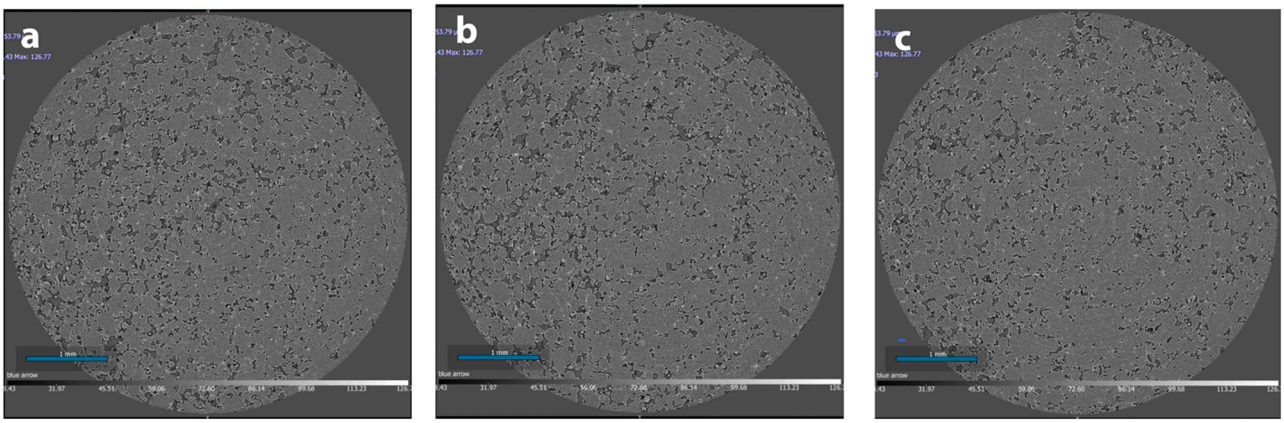

Fig. 5. NanoCT of the biphasic porous structure: cross-sectional images from the bottom (a), middle (b) and top (c) of the sample (scale bar = 1 mm).

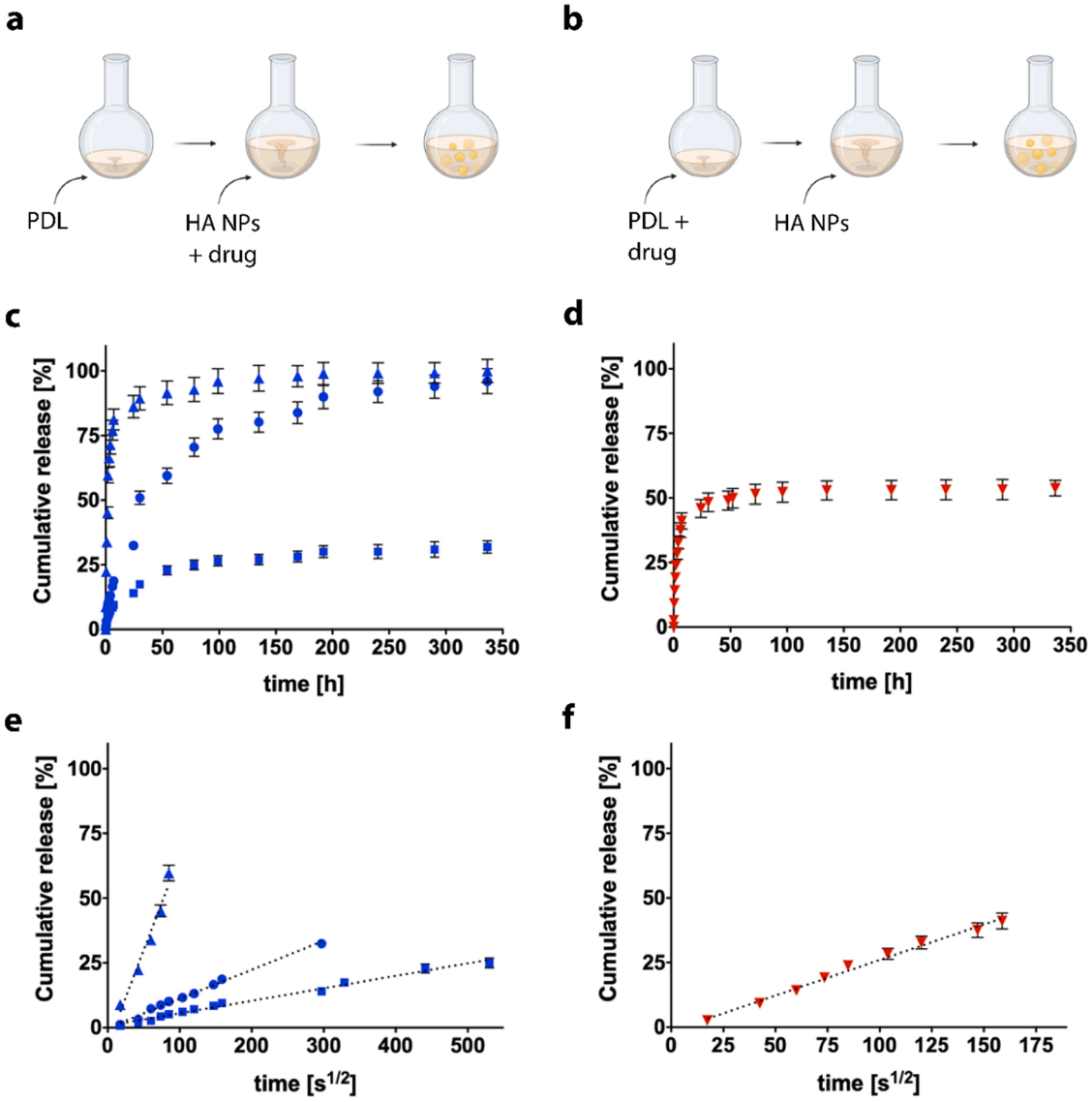

Fig. 6. a, b) Loading procedures for hydrophilic and hydrophobic drugs during device formation. c) In vitro release profile of different fluorescent delivered from biphasic porous structure (sodium fluorescein, triangle; dextran 10 kDa, circles; dextran 70 kDa, squares). d) In vitro release profile of FITC delivered from biphasic porous structure. e, f) The slope of drug release against the square root of time is representative of Fickian diffusion coefficients for each sample ($p < 0.001$ between all groups). Cumulative release (%) is calculated relative to the amount of drug loaded ($n = 3$, mean ± standard deviation).

structure.

The release of all drugs are prolonged with time depending on the molecular weight (Fig. 6c) and affinity with water (Fig. 6d). In particular, from Fig. 6c is evident that hydrophilic drug mimetic with low molecular weight (sodium fluorescein, triangle) shows a quicker release kinetics (higher slope vs time) due to the high affinity with the outer aqueous phase and lower steric hindrance. As expected increasing the steric hindrance of the drug molecules loaded it is possible to observe slower release kinetics (10 kDa, circles; 70 kDa, squares). On the contrary, low molecular weight hydrophobic drug, FITC, comparable with sodium fluorescein, present a slower release due to the low affinity with the releasing medium. One key problem in nanomedicine is the burst release [42], instantaneous loss of matter when delivery systems meet water environment: this was not observed in any cases for the biphasic system. The release started with Fickian diffusion followed by a plateau. The presence of Fickian diffusion, a condition desirable in drug delivery [43,44], is evident from Fig. 6e and f where a linear relationship is observed between the percentage released and the square root of time [45]. The duration of Fickian diffusion depends on the affinity with water (higher for hydrophobic molecules) and on the molecular weight of the molecules loaded (higher increasing the hindrance). It is possible to state that the biphasic structures produced can sustain the release of high and low molecular weight drugs, the latter high susceptible to uncontrolled kinetics and burst release.

4. Conclusions

In this work we demonstrated how colloidal nanoparticles can place at the interface between monomer and water in equal volumes without affecting bulk polymerization. This can ensure the formation of a biphasic structure stable (absence of phase separation) that can be used as drug delivery system both for hydrophilic and hydrophobic drugs. Other applications are indeed feasible due to the system's high porosity. The presence of nanoparticles can efficiently stabilize the device without using tensides nor organic solvent with a straightforward procedure that can be applied in many other systems.

CRediT authorship contribution statement

Alessandra Partenope: Methodology, Validation, Writing – original draft. **Fabio Pizzetti**: Methodology, Validation, Writing – original draft. **Valeria Vanoli**: Methodology, Validation. **Mosè Casalegno**: Investigation, Validation. **Alberto Cingolani**: Conceptualization. **Liebert Parreiras Nogueira**: Methodology. **Franca Castiglione**: Investigation, Validation. **Håvard J. Haugen**: Methodology. **Filippo Rossi**: Conceptualization, Supervision, Writing – review & editing.

Declaration of Competing Interest

The authors declare the following financial interests/personal relationships which may be considered as potential competing interests: Filippo Rossi reports financial support was provided by Polytechnic of Milan.

Data availability

The raw data required to reproduce these findings are available to download from https://data.mendeley.com/v1/datasets/publish-confirmation/mmwjfby936/1.

Acknowledgements

Authors would like to acknowledge Prof. Alessandro Sacchetti, Dr. Arianna Rossetti, Mr. Øystein Øvrebø and Mr. Alessandro Marchetti for fruitful discussion.

Appendix A. Supporting information

Supplementary data associated with this article can be found in the online version at doi:10.1016/j.mtcomm.2022.104290.

References

[1] S.Y. Lin, C.S. Chern, T.J. Hsu, I. Capek, Emulsion polymerization of styrene: double emulsion effect, Polymer 42 (4) (2001) 1481–1491.
[2] C. Solans, P. Izquierdo, J. Nolla, N. Azermanr, M.J. Garcia-Celma, Nano-emulsions, Curr. Opin. Colloid Interface Sci. 10 (3–4) (2005) 102–110.
[3] A. Chaudhari, Y. Pan, N. Nitin, Beverage emulsions: comparison among nanoparticle stabilized emulsion with starch and surfactant stabilized emulsions, Food Res. Int. 69 (2015) 156–163.
[4] J.M. Hohlfeld, The role of surfactant in asthma, Respir. Res. 3 (2001) 4.
[5] B. Gabard, E. Chatelain, E. Bieli, S. Haas, Surfactant irritation: in vitro corneosurfametry and in vivo bioengineering, Ski. Res. Technol. 7 (1) (2008) 49–55.
[6] S.U. Pickering, Emulsions, J. Chem. Soc. Trans. 91 (1907) 2001–2021.
[7] S. Sacanna, W.K. Kegel, A.P. Philipse, Thermodynamically stable pickering emulsions, Phys. Rev. Lett. 98 (2007), 158301.
[8] N. Xue, G. Zhang, X. Zhang, H. Yang, A reinforced Pickering emulsion for cascade reactions, Chem. Commun. 2018 (2018) 54.
[9] J. Zhang, X. Ge, M. Wang, J. Yang, Q. Wu, M. Wu, N. Liu, Z. Jin, Hybrid hollow microspheres templated from double Pickering emulsions, Chem. Commun. 46 (2010) 4318–4320.
[10] B.M. Trinh, M. Smith, T.H. Mekonnen, A nanomaterial-stabilized starch-beeswax Pickering emulsion coating to extend produce shelf-life, Chem. Eng. J. 431 (2022), 133905.
[11] H. Meng, D. Du, Pickering emulsions stabilized by ultrashort nanotubes, Mater. Today Chem. 20 (2021), 100436.
[12] J. Xu, A. Ma, T. Liu, C. Lu, D. Wang, H. Xu, Janus-like Pickering emulsions and their controllable coalescence, Chem. Commun. 49 (2013) 10871–10873.
[13] J. Frelichowska, M.A. Bolzinger, Y. Chevalier, Pickering emulsions with bare silica, Coll. Surf. 343 (1–3) (2009) 70–74.
[14] M.F. Haase, N. Sharifi-Mood, D. Lee, K.J. Stebe, In situ mechanical testing of nanostructured bijel fibers, ACS Nano 10 (6) (2016) 6338–6344.
[15] M.F. Haase, K.J. Stebe, D. Lee, Continuous fabrication of hierarchical and asymmetric bijel microparticles, fibers, and membranes by solvent transfer-induced phase separation (STRIPS), Adv. Mater. 27 (44) (2015) 7065–7068.
[16] C. Wu, C.L. Wang, L. Sun, K.M. Xu, W.Y. Zhong, PLGA nanoparticle-reinforced supramolecular peptide hydrogels for local delivery of multiple drugs with enhanced synergism, Soft Matter 16 (46) (2020) 10528–10536.
[17] R.X. Jia, L.S. Teng, L.Y. Gao, T. Su, L. Fu, Z.D. Qiu, Y. Bi, Advances in multiple stimuli-responsive drug-delivery systems for cancer therapy, Int. J. Nanomed. 16 (2021) 1525–1551.
[18] F. Pinelli, M. Saadati, E.N. Zare, P. Makvandi, M. Masi, A. Sacchetti, F. Rossi, A perspective on the applications of functionalized nanogels: promises and challenges, Int. Mater. Rev. (2022), https://doi.org/10.1080/09506608.2022.2026864.
[19] F. Pizzetti, A. Rossetti, A. Marchetti, F. Castiglione, V. Vanoli, E. Coste, V. Veneruso, P. Veglianese, A. Sacchetti, A. Cingolani, F. Rossi, Biphasic porous structures formed by monomer/water interface stabilization with colloidal nanoparticles, Adv. Mater. Interfaces 8 (2021) 2100991.
[20] M.E. Cates, P.S. Clegg, Bijels: a new class of soft materials, Soft Matter 4 (2008) 2132.
[21] S.B. Di, X. Liu, D. Liu, T. Gong, L.X. Lu, S.B. Zhou, A multifunctional porous scaffold with capacities of minimally invasive implantation, self-fitting and drug deliver, Mater. Today Chem. 1–2 (2016) 52–62.
[22] W. Yuan, L. Zhou, Z. Zhang, Y. Ying, W. Fan, K. Chai, Z. Zhao, Z. Tan, F. Shen, H. Ji, Synergistic dual-functionalities of starch-grafted-styrene hydrophilic porous resin for efficiently removing bisphenols from wastewater, Chem. Eng. J. 429 (2022), 132350.
[23] A.Y. Al-Maharma, S.P. Patil, B. Markert, Effects of porosity on the mechanical properties of additively manufactured components: a critical review, Mater. Res. Express 7 (2020) 12.
[24] J. Gallagher, The importance of being porous, Nat. Energy 4 (2019) 630.
[25] A. Kulkarni, S.C. Jana, Surfactant-free syndiotactic polystyrene aerogel foams via Pickering emulsion, Polymer 212 (2021), 123125.
[26] X. Yiang, Z. Yin, X. Zhang, Y. Zhu, S. Zhang, Fabrication of emulsion-templated macroporous poly(ε-caprolactone) towards highly effective and sustainable oil/water separation, Polymer 204 (2020), 122852.
[27] H. Gui, T. Zhang, Q. Guo, Nanofibrous, emulsion-templated syndiotactic polystyrenes with superhydrophobicity for oil spill cleanup, ACS Appl. Mater. Interfaces 11 (2019) 36063–36072.
[28] V. Ladelta, P. Bilalis, Y. Gnanou, N. Hadjichristidis, Ring-opening polymerization of ω-pentadecalactone catalyzed by phosphazene superbases, Polym. Chem. 8 (2017) 511–515.
[29] A. Kumar, B. Kalra, A. Dekhterman, R.A. Gross, Efficient ring-opening polymerization and copolymerization of ε-caprolactone and ω-pentadecalactone catalyzed by Candida antartica Lipase B, Macromolecules 33 (2000) 6303–6309.
[30] A. Kumar, K.H. Prakash, P. Cheang, K.A. Khor, Temperature driven morphological changes of chemically precipitated hydroxyapatite nanoparticles, Langmuir 20 (13) (2004) 5196–5200.

[31] D.A. Ossipov, S. Piskounova, O.P. Varghese, J. Hilborn, Functionalization of hyaluronic acid with chemoselective groups via a disulfide-based protection strategy for in situ formation of mechanically stable hydrogels, Biomacromolecules 11 (9) (2010) 2247–2254.
[32] K. Czifrak, C. Lakatos, M.A. Kordovan, L. Nagy, L. Daroczi, M. Zsuga, S. Keki, Block copolymers of poly(ω-pentadecalactone) in segmented polyurethanes: novel biodegradable shape memory polyurethanes, Polymers 12 (2020) 1928.
[33] V.B. Carmona, A.C. Correa, J.M. Marconcini, C.M.L. H, Properties of a biodegradable ternary blend of thermoplastic starch (TPS), Poly(ε-Caprolactone) (PCL) and Poly(Lactic Acid) (PLA), J. Polym. Environ. 23 (2015) 83–89.
[34] D.V. Deshmukh, N. Pasquero, G. Rathore, J. Zvick, O. Bar-Nur, J. Dual, M. W. Tibbitt, Screening method to identify hydrogel formulations that facilitate myotube formation from encapsulated primary myoblasts, Bioeng. Transl. Med. 5 (3) (2020).
[35] J.A. Shadish, G.M. Benuska, C.A. DeForest, Bioactive site-specifically modified proteins for 4d patterning of gel biomaterials, Nat. Mater. 18 (2022) 1005–1014.
[36] N.R. Richbourg, N.A. Peppas, The swollen polymer network hypothesis: quantitative models of hydrogel swelling, stiffness, and solute transport, Prog. Polym. Sci. 105 (2020), 101243.
[37] B.V. Slaughter, S.S. Khurshid, O.Z. Fisher, A. Khademhosseini, N.A. Peppas, Hydrogels in regenerative medicine, Adv. Mater. 21 (32–33) (2009) 3307–3329.
[38] E.O. Stejskal, J.E. Tanner, Spin diffusion measurements: spin echoes in the presence of a time-dependent field gradient, J. Chem. Phys. 42 (1965) 288.
[39] F. Castiglione, M. Casalegno, M. Ferro, F. Rossi, G. Raos, A. Mele, Evidence of superdiffusive nanoscale motion in anionic polymeric hydrogels: analysis of PGSE-NMR data and comparison with drug release properties, J. Control. Release 305 (2019) 110–119.
[40] S. Koutsopoulos, L.D. Unsworth, Y. Nagai, S. Zhang, Controlled release of functional proteins through designer self-assembling peptide nano!ber hydrogel scaffold, Proc. Natl. Acad. Sci. USA 106 (2009) 4623–4628.
[41] G. Perale, F. Rossi, M. Santoro, M. Peviani, S. Papa, D. Llupi, P. Torriani, E. Micotti, S. Previdi, L. Cervo, E. Sundstrom, A.R. Boccaccini, M. Masi, G. Forloni, P. Veglianese, Multiple drug delivery hydrogel system for spinal cord injury repair strategies, J. Control. Release 159 (2012) 271–280.
[42] X. Huang, C.S. Brazel, On the importance and mechanisms of burst release in matrix-controlled drug delivery systems, J. Control. Release 73 (2–3) (2001) 121–136.
[43] Y. Fu, W.J. Kao, Drug release kinetics and transport mechanisms of non-degradable and degradable polymeric delivery systems, Expert Opin. Drug Deliv. 7 (4) (2010) 429–444.
[44] J.M. Unagolla, A.C. Jayasuriya, Drug transport mechanisms and in vitro release kinetics of vancomycin encapsulated chitosan-alginate polyelectrolyte microparticles as a controlled drug delivery system, Eur. J. Pharm. Sci. 114 (2018) 199–209.
[45] K. Vulic, M. Shoichet, Tunable growth factor delivery from injectable hydrogels for tissue engineering, J. Am. Chem. Soc. 134 (2) (2012) 882–885.